

Joint ISAR Imaging and Phase Error Correction Based on Sparse Bayesian Learning

Wuge Su, Yuliang Qin, Hongqiang Wang, and Qi Yang

School of Electronic Science and Engineering, National University of Defense Technology, Changsha 410073, China

Email: suwuge_zhanlang@sina.com

Abstract—The ISAR imaging algorithm has depend on the mathematical model of the observation process, and the inaccuracies in the observation model may cause the model errors. In this paper, ISAR imaging is regarded as a narrow-band version of the Computer Aided Tomography (CT), where the phase errors in ISAR data are treated as model errors. Based on the inherent sparsity of targets in the imaging area, the ISAR imaging joint with phase adjustment is represented by a sparse signal reconstruction problem, which is set up as an optimization problem in a Sparse Bayesian Learning (SBL) framework. Owing to the superiority of the SBL, we employ an expansion-compression variance-component based method (ExCoV) to reconstruct the target's scattering coefficients and correct the phase error alternately via the maximum likelihood estimation. The numerical simulation results show the effectiveness of this novel method for various types of phase errors, which can produce a relatively well-focused image of the target and obtains the improvements over existing techniques for model error compensation in ISAR.

Index Terms—ISAR imaging, computer aided tomography, phase error correction, sparse Bayesian learning, ExCoV

I. INTRODUCTION

As a widely used remote sensor, the radar can obtain high resolution images of non-cooperative moving targets at long distance. Due to the advantages of robust performance under all-weather circumstance and high probability of target recognition, the Inverse Synthetic Aperture Radar (ISAR) is a candidate tool in many military and civilian applications, such as the air/space surveillance and the aircraft traffic control. However, the traditional imaging algorithms based on match filter, usually suffer from the low resolution and high sidelobes. Lots of high resolution ISAR imaging algorithms have been proposed to deal with such problem. Recently, there has been significant and increasing interest in addressing the sparse signal reconstruction in Radar imaging [1]. In particular, based on the sparse of signal, the Compressive Sensing (CS) has been extensively studied and successfully applied in ISAR image reconstruction [2].

The ISAR imaging model can be represented by the tomography [3], which is in light of the Computer Aided Tomography (CT) imaging technique [4], [5]. The word tomography, which means reconstruction from slices and

the turntable targets imaging formula based on the projection-slice theorem. Under the CT frame, the ISAR image formation can be represented by an inverse problem. CS has emerged as a promising technique to solve the inverse problem in ISAR imaging. Based on the echo of radar signal is parsimonious, the scatter coefficients of target can be recovered from the high-dimensional through a low-dimensional projection. However, the solution of inverse problems in ISAR imaging requires the use of precise mathematical model in the observation process and these techniques based on CS theory rely on the assumption that there has no residual phase error in the processed data. In ISAR imaging, the relative motion between the radar and target can be decomposed into translational and rotational motions, but only the rotational motion of the target contributes to the formation of the Doppler spectrum. The rotational motion-induced errors cause the phase errors, which are main reasons for model uncertainties. For most of the Range Doppler (RD) or CS-based ISAR imaging algorithm [6]-[8], the translation motion is presumed to be perfectly compensated. However, such uncertainties often result the phase errors and suffer the undesired artifacts in the formed ISAR image, then the autofocus techniques are developed for solve this type of problem.

The conventional autofocus techniques, such as map-drift autofocus [9], Phase Gradient Autofocus (PGA) [10] and Minimum-Entropy Method (MEM) [11], which based on the observation mathematical model in ISAR are accurate and belong to the post-processing approaches. Although these autofocus techniques are simple to implement and computationally efficient, they usually suffer from high sidelobe levels which visually smears the target signature and cannot be easy integrated into the CS framework to estimate the phase error and obtain the high focus target ISAR image.

According to the Geometrical Theory of Diffraction (GTD) theory [12], for high-resolution images at high frequencies, the scattering responses of an object can be well approximated as a sum of responses from individual reflectors, and the echo of the ISAR target can be represented by a few individual scatters, then the echo of ISAR targets can be formulated as a sparse signal representation problem [13], [14]. Various studies have been presented on the phase error correction in ISAR imaging which are considered by the sparse recover problems [15], [16]. These methods make use of the

knowledge of object sparsity, which has been shown to offer certain improvements over conventional imaging. Through it satisfies an appropriate phase error model, the use of sparse representation aims at the minimization of the l_1 -norm to reconstruct the target scatter coefficients [15]. Nevertheless, the l_1 -norm minimization is sensitive to user parameters which are typically functions of the noise or signal sparsity levels and require tuning. Setting the user parameters is not trivial and the reconstruction performance depends crucially on their choices [17]. To overcome this disadvantage, the sparse recovery scheme is interpreted by using the Bayesian philosophy in [18], however, the phase adjustment is realized by solving the optimization based on Hessian update scheme, which needs more computational cost.

The sparse Bayesian recover algorithm employs a sparse prior on the signal, and estimates the parameter based on the Bayesian inference [18]. Moreover, the sparse Bayesian recover algorithm is automatic and does not require tuning or knowledge of signal sparsity or noise levels. The most popular sparse Bayesian approaches, include Sparse Bayesian Learning (SBL) [19], [20] and Bayesian Compressive Sensing (BCS) [21], are based on SBL model. Own to its priority, the SBL model is used in SAR/ISAR imaging and obtain high resolution radar images [8], [22]. In [23], based on the idea of the SBL methods, a multi-task Bayesian model is utilized in a hierarchical manner to the autofocused ISAR imaging problem and the result can produce a well-focused ISAR image. The major shortcomings of SBL are its high computational complexity and large memory requirements, which make its application on large-scale data practically impossible. In this paper, we use a sparse Bayesian recovering algorithm named ExCoV (expansion compression variance-component based method) [24] to ISAR imaging, which generalizes the SBL model and has a much smaller number of parameters to estimate than SBL. Because of its parsimony of the probabilistic model, the ExCoV is typically significantly faster than SBL [24], [25]. Motivated by the existed methods and the sparse echo of ISAR under the frame of CT, we develop an approach of iterative ExCoV via MLE (maximum likelihood estimation) for the joint ISAR imaging and phase error correction. The proposed ExCoV-MLE method handles the autofocus problem as an optimization problem, the ExCoV-MLE method is iteratively minimized the cost function with respect to the target scatter coefficients and the phase error. Firstly, the cost function is minimized with respect to the target scatter coefficients. Secondly, the phase error is estimated by MLE method, which is used to update the model matrix and the algorithm passes to the next iteration.

The rest of this paper is organized as follows. In Section 2, the sparse ISAR imaging model under the CT frame is introduced. The proposed method is described in detail in Section 3. Numerical simulations in Section 4 compare the imaging performances of the proposed and existing methods. Concluding remarks and future work are given in Section 5.

II. THE SPARSE ECHO OF ISAR OBSERVATION MODEL

In this section, in terms of the projection slice theorem [3], [4], ISAR imaging can be regarded as a narrow-band version of CT under the far-field scenario. In light of the CT image reconstruction, the geometry of ISAR principle is illustrated in Fig. 1. In the following, the mathematical model of ISAR imaging model with the phase error under the CT frame is formulated.

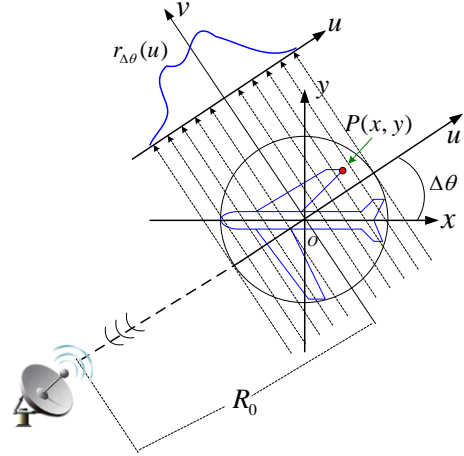


Figure 1. The tomography geometry for data collection in ISAR

In Fig. 1, the coordinate $u-o-v$ is immobile to the radar and the coordinate $x-o-y$ is fixed on the target.

The relation of two coordinate is respectively as:

$$\begin{cases} u = x \cos \Delta\theta + y \sin \Delta\theta \\ v = -x \sin \Delta\theta + y \cos \Delta\theta \end{cases} \quad (1)$$

$$\begin{cases} x = u \cos \Delta\theta - v \sin \Delta\theta \\ y = u \sin \Delta\theta + v \cos \Delta\theta \end{cases} \quad (2)$$

where $\Delta\theta$ is the rotation angle of target around the center o from counterclockwise rotation. From Fig. 1, during the CPI (coherent processing interval), the instantaneous rotation angle of the target is defined as $\Delta\theta(t_m)$, where t_m is the slow time, the instantaneous range from the random scatter center at $P(x, y)$ to radar is given by $R(t_m) = R_0 + y \cos \Delta\theta(t_m) + x \sin \Delta\theta(t_m)$, where R_0 is the distance from the radar to the center of plane. Then the instantaneous range between the point scatter $P(x, y)$ and the reference point O is:

$$R_{\Delta}(t_m) = y \cos \Delta\theta(t_m) + x \sin \Delta\theta(t_m) \quad (3)$$

In ISAR systems, one of the most widely used signals is the linear frequency modulated (LFM) signal, which is often used for high resolution and a long coherent processing interval. In this paper, we defined the emitted LFM signal is:

$$s(\hat{t}) = \text{rect}\left(\frac{\hat{t}}{T_p}\right) \cdot \exp\left[j2\pi\left(f_c \hat{t} + \frac{\gamma}{2} \hat{t}^2\right)\right] \quad (4)$$

where $\text{rect}(\hat{t}/T_p)$ represents the window function, T_p denotes the pulse duration, the chirp rate is $\gamma = B/T_p$, B represents the bandwidth, \hat{t} is the fast time and f_c is the

centered frequency. Then the received signal from a random scatter in target at a distance of R can be simply written as:

$$s(\hat{t}, \theta) = \iint_{\Omega} \sigma(x, y) s(\hat{t} - \frac{2R}{c}) dx dy \quad (5)$$

where Ω is the integration area of reflected signals. For a given observation angle θ , $\sigma(x, y)$ is a complex function and models the reflectivity density of the target at (x, y) in the scattering field. A common sense is that when an arbitrary target is illuminated by a radar, the backscattered signal will consist of the superposition of the returns from a multitude of scattering centers just like in the CT imaging.

The relationship $r_{\Delta\theta}(u) = \int_{(\theta, u) \text{ line}} \sigma(x, y) ds$ is used to define line integral $r_{\Delta\theta}(u)$ in Fig. 1. The relationship between the projection $r_{\Delta\theta}(u)$ and the scatter $\sigma(x, y)$ can be represented as:

$$r_{\Delta\theta}(u) = \iint_{\Omega} \sigma(x, y) \delta(u - x \cos \Delta\theta - y \sin \Delta\theta) dx dy \quad (6)$$

where $r_{\Delta\theta}(u)$ is actually the Radon transform of $\sigma(x, y)$ along the radar line of sight $\Delta\theta$. Without loss of generality, in order to reduce the received effective bandwidth, the dechirp method is employed. After coherent processing, we obtain the complex envelope of the return echo from the target and take account of the phase errors as:

$$\begin{aligned} \tilde{s}(\hat{t}, \Delta\theta) &= \int_u r_{\Delta\theta}(u) \exp(j\varphi) s(\hat{t} - \frac{2R(t_m)}{c}) du \\ &= \int_u r_{\Delta\theta}(u) \exp(j\varphi) \exp\{j\int_{f_0} \tilde{f}_0(\hat{t} - \frac{2R(t_m)}{c} \\ &\quad + \alpha(\hat{t} - \frac{2R(t_m)}{c})^2)\} du \end{aligned} \quad (7)$$

After mixing, low-pass filtering, it can be approximately obtained as follows:

$$\tilde{s}(\hat{t}, \theta) = \int_u r_{\Delta\theta}(u) \exp(j\varphi) \exp\{-jk(\hat{t})u\} du \quad (8)$$

where $k = 2(f_c + \gamma\hat{t})/c$ denotes the spatial frequency variable. From (8), it can be seen that the returned signal can be identified as the Fourier transform of the projection $r_{\Delta\theta}(u)$, this is the core idea of projection-slice theorem in CT imaging. Substituting (6) into (8), the relationship between the object scatter reflectivity $\sigma(x, y)$ and the demodulated observed signal $\tilde{s}(\hat{t}, \Delta\theta)$ can be represented as:

$$\tilde{s}(\hat{t}, \Delta\theta) = \iint_{\Omega} \sigma(x, y) \exp(j\varphi) \exp\{-jk(\hat{t}) \cdot (x \cos \Delta\theta + y \sin \Delta\theta)\} dx dy \quad (9)$$

Supposing the ISAR works at high frequencies and according to the geometric theory of diffraction, the tomographic ISAR echo data related to (9) can be represented by:

$$S(t, \theta) = \sum_i \sigma_i(x, y) \exp(j\varphi_m) \exp[-jk(t)R_{\Delta}(t_m)] + \varepsilon(\hat{t}) \quad (10)$$

where I is the number of the strongest scattering centers in ISAR target. The noise $\varepsilon(\hat{t})$ is assumed complex Gaussian with power spectral density σ_{ε}^2 and is assumed to be independent for different range bin.

We discretize the ISAR imaging area into a grid of uniform cells where each of the target scatters is located at one of cells. Based on the ISAR scene geometry and the data formation above, the sparse presentation model can be derived as follows. Let M_1 and M_2 denote the number of image grid points in the X and Y directions, N_1 and N_2 denote the number of fast time grid points and the number of observing angle grid points, respectively. The total number of unknowns is $M = M_1 \times M_2$ and the total number of the observed data points is $N = N_1 \times N_2$. For a scatter located at (x_k, y_l) , the N -element steering vector can be written as:

$$\mathbf{a}_{k,l} = [b_{k,l}(1,1), \dots, b_{k,l}(1, N_2), \dots, b_{k,l}(N_1, 1), \dots, b_{k,l}(N_1, N_2)]^T \quad (11)$$

where $b_{k,l}(p, q) = \exp(-jk(\hat{t}_p)(y_k \cos \Delta\theta_q + x_l \sin \Delta\theta_q))$, $1 \leq p \leq N_1$, $1 \leq q \leq N_2$, $1 \leq k \leq M_1$, $1 \leq l \leq M_2$. Then, the steering matrix can be written as:

$$\mathbf{A} = [\mathbf{a}_{1,1}, \dots, \mathbf{a}_{M_1,1}, \dots, \mathbf{a}_{1,M_2}, \dots, \mathbf{a}_{M_1,M_2}] \quad (12)$$

The phase error matrix is denoted by $\mathbf{E} = \text{diag}\{\exp(j\varphi_1), \dots, \exp(j\varphi_N)\}$ and the complex ISAR imagery is denoted by:

$$\boldsymbol{\sigma} = [\sigma(x_1, y_1), \dots, \sigma(x_1, y_{M_2}), \dots, \sigma(x_{M_1}, y_1), \dots, \sigma(x_{M_1}, y_{M_2})]^T \quad (13)$$

The received radar data are stacked into the vector \mathbf{s} , then the ISAR imaging mathematical model with phase error can be given in matrix form as

$$\mathbf{s} = \mathbf{E}\mathbf{A}\boldsymbol{\sigma} + \boldsymbol{\varepsilon} \quad (14)$$

where $\mathbf{s} \in N \times 1$ and $\boldsymbol{\varepsilon}$ represents the additive zero-mean complex Gaussian noise matrix.

III. AUTOFOCUS TECHNIQUE BASED ON EXCOV-MLE METHOD

The autofocus technique includes mainly two stages. Firstly, defining (i) as the counter of iteration and assuming the i th estimations are obtained, we alternatively optimize $\hat{\sigma}^{(i+1)}$ and the phase errors $\hat{\mathbf{E}}^{(i+1)}$ in the $(i+1)$ th iteration. The detailed algorithm is stated as follows.

A. Update the $\hat{\sigma}^{(i+1)}$ by ExCoV Method [24], [25]

We assumed the $\hat{\mathbf{E}}^{(i)}$ is obtained, and $\hat{\mathbf{H}}^{(i)} = \hat{\mathbf{E}}^{(i)}\mathbf{A}$. The ExCoV method use the GML rule to select the best index set Ω , and the GML rule maximizes $\text{GML}(\Omega) = \text{GL}(\Omega, \hat{\rho}_{\Omega})$, here the $\hat{\rho}_{\Omega} = (\hat{\boldsymbol{\xi}}_{\Omega}, \hat{\gamma}^2, \hat{\delta}^2(\Omega))$ = arg max $\text{In } p(\mathbf{s} | \boldsymbol{\theta})$ is the ML estimate of ρ_{Ω} for given Ω , and $\text{GL}(\boldsymbol{\theta}) = \text{In } p(\mathbf{s} | \boldsymbol{\theta}) - |\Gamma(\boldsymbol{\theta})|/2$, where $\Gamma(\boldsymbol{\theta})$ is

the Fisher information matrix (FIM) for the signal variance components ξ_Ω and γ^2 . The $\Gamma(\theta)$ is defined in Appendix A and it can be penalizes the growth of Ω . The GML rule thereby balances modeling accuracy and efficiency.

The basic idea of the ExCoV is to interleave the two steps that approximately maximizes GML rule, which contains multiple cycles. One of step is the expansion and compression steps with goal to find a more efficient Ω ; For a fixed Ω , the other step is the Expectation-Maximization (EM) steps, thereby approximating $\hat{\rho}_\Omega$. The best estimate of θ and corresponding signal estimate obtained in the entire history of the algorithm.

B. Update the $\hat{\mathbf{E}}^{(i+1)}$ by Maximum Likelihood Estimation (MLE)

Since no prior for phase error matrix $\hat{\mathbf{E}}^{(i+1)}$ is available, the inference of $\hat{\mathbf{E}}^{(i+1)}$ can be obtained by MLE method. Suppose we obtain the best estimate of $\hat{\sigma}^{(i+1)}$ in ExCoV algorithm, the solution of elements in $\hat{\mathbf{E}}^{(i+1)}$ can be formulated by minimizing the negative log-likelihood function as:

$$\hat{\varphi}_m^{(i+1)} = \arg \min_{\varphi_m} \|s - \exp(j\varphi_m) \mathbf{A} \hat{\sigma}^{(i+1)}\|_2^2, \quad m=1, \dots, M \quad (15)$$

The above problem is a convex optimization problem and having a closed-form solution. We set the derivative with respect to φ_m to zero (see Appendix B for details) and we can obtain:

$$\hat{\varphi}_m^{(i+1)} = \arctan \left(\frac{\text{Im}\{(\hat{\sigma}^{(i+1)})^H \mathbf{A}^H s\}}{\text{Re}\{(\hat{\sigma}^{(i+1)})^H \mathbf{A}^H s\}} \right) \quad (16)$$

We repeat the two stages above until the ExCoV-MLE shows no obvious improvement.

IV. NUMERICAL SIMULATIONS

In this section, we present several numerical simulation results using synthetic and electromagnetically calculation data to illustrate the performance of the proposed algorithm. Some popular methods are also presented.

A. Synthetic Data Experiments

Suppose radar transmits LFM signal with bandwidth 1GHz and carry frequency 10GHz. The sampling number in fast time is 256, and the observation azimuth varies within $-2.5^\circ \sim 2.5^\circ$, corresponding sampling number is 512. The imaging target is composed of 23 scattering centers, as shown in Fig. 2. The width of scene is 10m in both azimuth and range and the sampling space to reconstruct the sparse basis is 0.2m in both azimuth and range. Three different types of phase errors (sinusoidal errors, quadratic errors, and uniformly distributed random errors), are simulated. In Fig. 3, radar echoes are generated according to the point scattering model and 0dB Gaussian complex noises are added. Based on CS theory, we randomly choose the 20 sampling point from the fast time and observation azimuth respectively and

use the proposed algorithms to reconstruct the ISAR images. The Monte Carlo number is set by 500 and the iteration number in phase error estimation is set by 10. In Fig. 3, the reconstructed target reflection coefficients are given to evaluate the proposed algorithm. Among all the imaging results, it is seen that ExCoV-MLE method can obtain a well-focused and precision ISAR image in low SNR, although one scatterer is lost in the random phase error scenario.

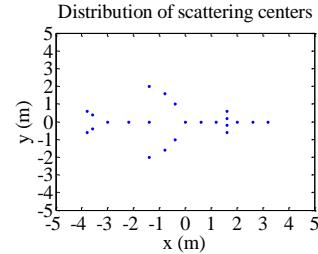


Figure 2. Reflectivity distribution of simulated target

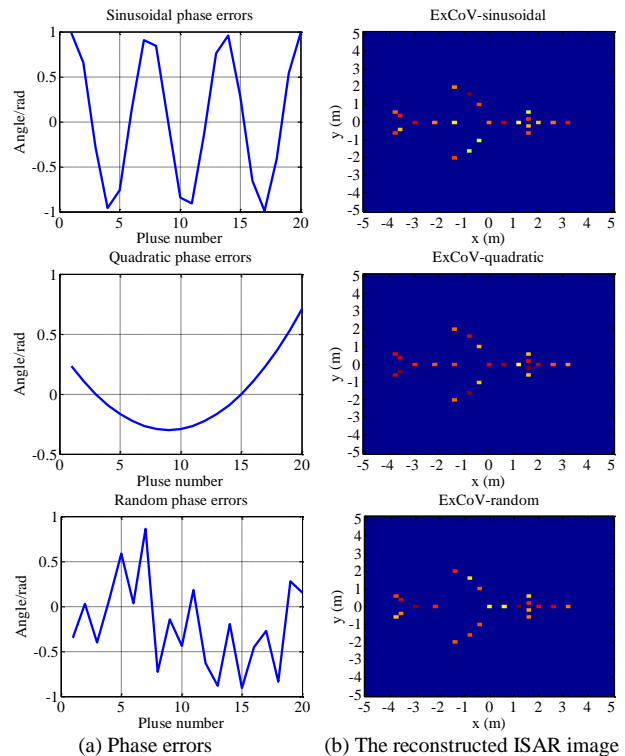


Figure 3. ISAR imaging result with SNR=0dB

The top figures are quadratic phase errors and the reconstructed ISAR image. The middle figures are the sinusoidal phase errors and the reconstructed ISAR image. The bottom figures are the random phase errors and the reconstructed ISAR image. In this paper, we define the MSE of sparse signal as the error between the reconstructed scatter coefficients and the true value, i.e., $\|\sigma_0 - \hat{\sigma}_i\| / \sigma_0$, where $\hat{\sigma}_i$ denotes the estimate of scatter coefficients in the i th iteration and σ_0 denotes the true value of scatter coefficients. We also define the MSE of phase errors as the error between the estimated phase errors and the true value, i.e., $\|\varphi_0 - \hat{\varphi}_i\| / \varphi_0$, where $\hat{\varphi}_i$ denotes the estimate of phase errors in the i th iteration

and φ_0 denotes the true value of phase errors. Fig. 4 indicates the convergence of the proposed method at the SNR=0dB. As shown in Fig. 4(a) and Fig. 4(b), during the whole iteration process, the MSE of the sparse coefficient $\hat{\sigma}$ and the phase errors keep decreasing after each iteration. In particular, the three types of phase errors can converge to some extent after 10 iterations. These results mean that the ExCoV-MLE method is capable of reconstructing the target scatter coefficients accurately and estimating the phase errors in low SNR.

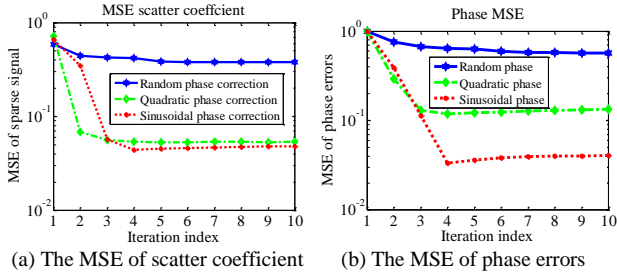


Figure 4. Convergence of the algorithm in terms of the iteration index

B. Electromagnetically Calculation Data Experiments

In the real environments, most of the object scatters are not located in the partition grids, causing the strong coherence of column in sparse dictionary. To validate the effectiveness of ExCoV-MLE algorithm in this situation, the Electromagnetic data which produced by the electromagnetism calculation software called CST 2014 are applied in this experiment.

We assume that the carrier frequency of the ideal signal is 10GHz, bandwidth is 1GHz, and that the sampling number of the frequency is 201. The azimuth angle is from 55 to 64.02, and the sampling number is 452. The type of the phase error is random the SNR is set to 3dB. As shown in Fig. 5, the measured target is a scaled model of F22 and its size is 9.2m \times 6.6m.

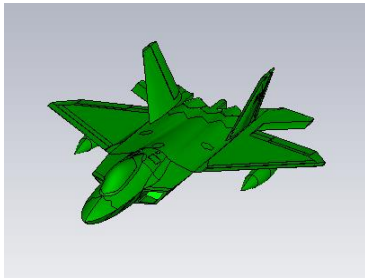


Figure 5. The F22 target model

Fig. 6(a), illustrates the imaging results of FFT methods with the full aperture data. It can be seen that the defocusing phenomenon and relatively high side lobes occur in azimuth direction. The imaging results of sparse recover algorithm which using a part of sampling data are shown in Fig. 6(b), Fig. 6(c) and Fig. 6(d). It can be seen that L1 and VBSBL based method have a relative degraded performance, While ExCoV-MLE method can greatly preserve the strong scatters and provides cleaner image. These advantages imply that ExCoV-MLE method is a better choice in joint ISAR imaging with phase error correction.

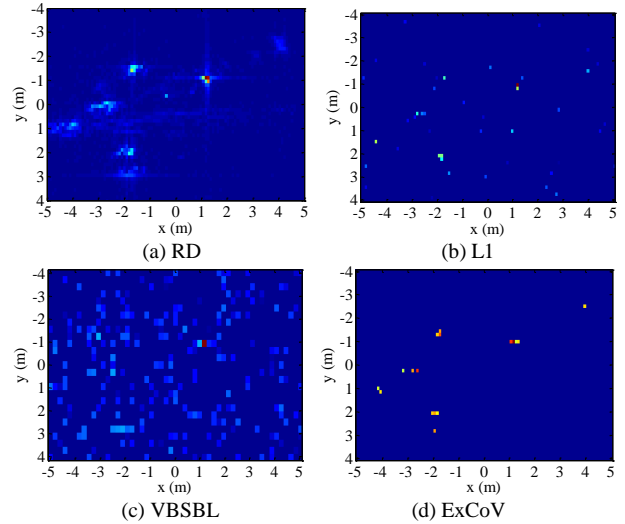


Figure 6. The imaging results of Electromagnetic Data

V. CONCLUSION

Due to the imperfection of coarse motion compensation, the phase error correction problem is considered in ISAR imaging. In this paper, the sparse ISAR imaging model is established based on CT frame and an efficient ISAR imaging with phase error correction method has been proposed based on the ExCoV-MLE method. The ExCoV-MLE alternately corrects the phase errors during the reconstruction of target reflection coefficients under the ExCoV framework. The ExCoV scheme is automatic and demands no prior knowledge about signal-sparsity or measurement-noise levels, which is suitable for large-scale problems. The simulation results show the effectiveness of the proposed approach as well as the improvements it provides over the existed methods. In addition, a well-focused image could also be achieved even under the condition of low SNR. However, since the computation load is another important issue for real-time ISAR imaging, an adaptive and fast ISAR imaging algorithm based on the sparse Bayesian recovery method is deserved to be explored in the future.

APPENDIX A

The compute of $\Gamma(\theta)$ using the FIM result for the Gaussian measurement model $\hat{\xi}_\Omega, \hat{\gamma}^2, \hat{\delta}^2$.

$$\Gamma(\theta) = \begin{bmatrix} \Gamma_{\xi_\Omega, \xi_\Omega}(\theta) & \Gamma_{\xi_\Omega, \gamma^2}(\theta) \\ \Gamma_{\xi_\Omega, \gamma^2}^T(\theta) & \Gamma_{\gamma^2, \gamma^2}(\theta) \end{bmatrix}$$

With each blocks in matrix $\Gamma(\theta)$ computed as follows:

$$\begin{aligned} \Gamma_{\xi_\Omega, \xi_\Omega}(\theta) &= \frac{1}{2} \left[\mathbf{H}_\Omega^T P(\theta) \mathbf{H}_\Omega \right] \odot \left[\mathbf{H}_\Omega^T P(\theta) \mathbf{H}_\Omega \right] \\ &= \frac{1}{2} \left[\mathbf{H}_\Omega^T P(\theta) \mathbf{H}_\Omega \right]^{\odot 2} \end{aligned}$$

$$\left[\Gamma_{\xi_\Omega, \gamma^2}^T(\theta) \right]_i = \frac{1}{2} \mathbf{H}_\Omega^T(:, i) P(\theta) \mathbf{H}_\Omega \mathbf{H}_\Omega^T P(\theta) \mathbf{H}_\Omega(:, i)$$

$$\Gamma_{\gamma^2, \gamma^2}(\theta) = \frac{1}{2} \text{tr} [P(\theta) \mathbf{H}_\Omega \mathbf{H}_\Omega^T P(\theta) \mathbf{H}_\Omega \mathbf{H}_\Omega^T]$$

where $i=1,2,\dots,m_\Omega$ and $\mathbf{H}_\Omega(:,i)$ denotes the i th column of \mathbf{H}_Ω .

APPENDIX B

The cost function for phase error estimation is as follows:

$$\hat{\varphi}_m^{(i+1)} = \arg \min_{\varphi_m} \left\| \mathbf{s} - \exp(j\varphi_m) \mathbf{A} \hat{\sigma}^{(i+1)} \right\|_2^2$$

We evaluate the norm expression and get by:

$$\begin{aligned} & \left\| \mathbf{s} - \exp(j\varphi_m^{(i+1)}) \mathbf{A} \hat{\sigma}^{(i+1)} \right\|_2^2 \\ &= \left\| \mathbf{s} - \exp(j\varphi_m^{(i+1)}) \mathbf{A} \hat{\sigma}^{(i+1)} \right\|^H \left\| \mathbf{s} - \exp(j\varphi_m^{(i+1)}) \mathbf{A} \hat{\sigma}^{(i+1)} \right\| \\ &= \mathbf{s}^H \mathbf{s} - \mathbf{s}^H \exp(j\varphi_m^{(i+1)}) \mathbf{A} \hat{\sigma}^{(i+1)} \\ &\quad - (\hat{\sigma}^{(i+1)})^H \mathbf{A}^H \exp(-j\varphi_m^{(i+1)}) \mathbf{s} \\ &\quad + (\hat{\sigma}^{(i+1)})^H \mathbf{A}^H \mathbf{A} \hat{\sigma}^{(i+1)} \\ &= \mathbf{s}^H \mathbf{s} - \mathbf{s}^H \left[\cos(\varphi_m^{(i+1)}) + j \sin(\varphi_m^{(i+1)}) \right] \mathbf{A} \hat{\sigma}^{(i+1)} \\ &\quad - (\hat{\sigma}^{(i+1)})^H \mathbf{A}^H \left[\cos(\varphi_m^{(i+1)}) - j \sin(\varphi_m^{(i+1)}) \right] \mathbf{s} \\ &\quad + (\hat{\sigma}^{(i+1)})^H \mathbf{A}^H \mathbf{A} \hat{\sigma}^{(i+1)} \\ &= \mathbf{s}^H \mathbf{s} - 2 \cos(\varphi_m^{(i+1)}) \operatorname{Re} \left\{ (\hat{\sigma}^{(i+1)})^H \mathbf{A}^H \mathbf{s} \right\} \\ &\quad - 2 \sin(\varphi_m^{(i+1)}) \operatorname{Im} \left\{ (\hat{\sigma}^{(i+1)})^H \mathbf{A}^H \mathbf{s} \right\} \\ &\quad + (\hat{\sigma}^{(i+1)})^H \mathbf{A}^H \mathbf{A} \hat{\sigma}^{(i+1)} \end{aligned}$$

By taking the derivative with respect to $\varphi_m^{(i+1)}$ and setting it to zero, we can obtain the result as shown in (7).

ACKNOWLEDGMENT

This work was supported by the National Natural Science Foundation of China (Grant No.61171133) and by the National Natural Science Foundation for Young Scientists of China (Grant No. 61101182, No. 61302148).

REFERENCES

[1] S. Samadi, M. Cetin, and M. A. Masnadi-Shirazi, "Sparse representation-based synthetic aperture radar imaging," *IET Radar Sonar Navig.*, vol. 5, no. 2, pp. 182-193, 2011.

[2] X. Du, C. W. Duan, and W. D. Hu, "Sparse representation based autofocusing technique for ISAR images," *IEEE Transactions on Geoscience and Remote Sensing*, vol. 3, no. 51, pp. 1826-1835, 2013.

[3] D. C. Munson, J. D. O'Brien, and W. K. Jenkins, "A tomographic formulation of spotlight-mode synthetic aperture radar," *Proceedings of the IEEE*, vol. 71, no. 8, pp. 917-925, 1983.

[4] A. C. Kak and M. Slaney, *Principles of Computerized Tomographic Imaging*, New York: IEEE Press, 1999.

[5] M. Cetin and W. C. Karl, "Feature-Enhanced synthetic aperture radar image formation based on nonquadratic regularization," *IEEE Transactions on Image Processing*, vol. 10, no. 4, pp. 623-631, 2001.

[6] X. H. Zhang, T. Bai, H. Y. Meng, and J. W. Cheng, "Compressive sensing based ISAR imaging via the combination of the sparsity and nonlocal total variation," *IEEE Geoscience and Remote Sensing Letters*, vol. 11, no. 5, pp. 990-994, 2014.

[7] L. Zhang, M. D. Xing, and C. W. Qiu, "Achieving higher resolution ISAR imaging with limited pulses via compressed sampling," *IEEE Geoscience and Remote Sensing Letters*, vol. 6, no. 3, pp. 567-571, 2009.

[8] H. C. Liu, B. Jiu, H. W. Liu, and Z. Bao, "Super resolution ISAR Imaging based on sparse Bayesian learning," *IEEE Transactions*

on Geoscience and Remote Sensing, vol. 52, no. 8, pp. 5005-5013, 2014.

[9] T. C. Calloway and G. Donohoe, "Subaperture autofocus for synthetic aperture radar," *IEEE Transactions on Aerospace and Electronic Systems*, vol. 30, no. 2, pp. 617-621, 1994.

[10] L. Yang, M. D. Xing, Y. Wang, L. Zhang, and Z. Bao, "Compensation for the NsRCM and phase error after polar format resampling for airborne spotlight SAR raw data of high resolution," *IEEE Geoscience and Remote Sensing Letters*, vol. 10, no. 1, pp. 165-169, 2013.

[11] L. Yang, M. Xing, L. Zhang, J. Sheng, and Z. Bao, "Entropy-Based motion error correction for high-resolution spotlight SAR imagery," *IET Radar Sonar and Navigation*, vol. 6, no. 7, pp. 627-637, 2012.

[12] M. J. Gertry, L. C. Potter, I. J. Gupta, and V. M. Andria, "A parametric model for synthetic aperture radar measurements," *IEEE Transactions on Antennas and Propagation*, vol. 47, no. 7, pp. 1179-1188, 1999.

[13] L. Zhang, Z. J. Qiao, M. D. Xing, J. L. Sheng, and Z. Bao, "High-Resolution ISAR imaging by exploiting sparse apertures," *IEEE Transactions on Antennas and Propagation*, vol. 60, no. 2, pp. 997-1008, 2012.

[14] G. Xu, M. D. Xing, L. Zhang, J. Duan, Q. Q. Chen, and Z. Bao, "Sparse apertures ISAR imaging and scaling for maneuvering targets," *IEEE Journal of Selected Topics in Applied Earth Observations and Remote Sensing*, vol. 7, no. 7, pp. 2942-2956, 2014.

[15] O. N. Önhon and M. Çetin, "A sparsity-driven approach for joint SAR imaging and phase error correction," *IEEE Transactions on Image Processing*, vol. 21, no. 4, pp. 2075-2088, 2012.

[16] G. Xu, M. D. Xing, L. Zhang, Y. B. Liu, and Y. C. Li, "Bayesian inverse synthetic aperture radar imaging," *IEEE Geoscience and Remote Sensing Letters*, vol. 8, no. 6, pp. 1150-1154, 2011.

[17] O. Batu and M. Çetin, "Parameter selection in sparsity-driven SAR imaging," *IEEE Transactions on Aerospace and Electronic Systems*, vol. 47, no. 4, pp. 3040-3050, 2011.

[18] A. Mohammad-Djafari, "Bayesian approach with prior models which enforce sparsity in signal and image processing," *EURASIP Journal on Advances in Signal Processing*, vol. 52, pp. 1-19, 2012.

[19] M. E. Tipping, "Sparse Bayesian learning and the relevance vector machine," *Journal of Machine Learning Research*, vol. 2, no. 1, pp. 211-244, 2001.

[20] D. P. Wipf and B. D. Rao, "Sparse Bayesian learning for basis selection," *IEEE Transactions on Signal Processing*, vol. 52, no. 8, pp. 2153-2164, 2004.

[21] S. H. Ji, Y. Xue, and L. Carin, "Bayesian compressive sensing," *IEEE Transactions on Signal Processing*, vol. 56, no. 6, pp. 2346-2356, 2008.

[22] J. Xu, Y. N. Pi, and Z. J. Cao, "Bayesian compressive sensing in synthetic aperture radar imaging," *IET Radar, Sonar and Navigation*, vol. 6, no. 1, pp. 2-8, 2012.

[23] L. F. Zhao, L. Wang, G. A. Bi, and L. Yang, "An autofocus technique for high-resolution inverse synthetic aperture radar imagery," *IEEE Transactions on Geoscience and Remote Sensing*, vol. 52, no. 10, pp. 6392-6403, 2014.

[24] K. Qiu and A. Dogandzic, "Variance-Component based sparse signal reconstruction and model selection," *IEEE Transactions on Signal Processing*, vol. 58, no. 6, pp. 2935-2952, 2010.

[25] A. Dogandzic and K. Qiu, ExCoV: Expansion-Compression variance-component based sparse-signal reconstruction from noisy measurements," in *Proc. 43rd Annual Conference Information Science and Systems*, Baltimore, USA, 2009, 186-191.



Wuge Su was born in Sichuan Province, China, in 1986. He received the B.S. and M.S. degree in control engineering from Aviation University Air Force, in 2008 and 2010, respectively. He received the Ph.D. degree in information and communication engineering from National University of Defense Technology in 2015. His research interests include optimum array processing, radar imaging technology and sparse Bayesian learning.



Yuliang Qin was born in Shandong Province, China, in 1980. He received his B.S., M.S., and Ph.D. degrees in information and communication engineering from National University of Defense Technology, Changsha, in 2002, 2004, and 2008, respectively. Currently, he is an Associate Professor at School of Electronic Science and Engineering, National University of Defense Technology. His research interests lie in the areas of radar

imaging and radar signal processing.



Qi Yang was born in Shaanxi Province, China, in 1989. He received the B.S. and M.S degrees in information and communication engineering from National University of Defense Technology, in 2012 and 2014, respectively. Since December, 2014, he has been a Ph.D. candidate at the National University of Defense Technology. His research interests include terahertz radar system and digital processing of ISAR.



Hongqiang Wang was born in Shaanxi Province, China, in 1970. He received his B.S., M.S., and Ph.D. degrees from National University of Defense Technology, Changsha, in 1993, 1999, and 2002, respectively. Currently, he is a Professor at School of Electronic Science and Engineering, National University of Defense Technology. He has been involved in modern radar signal processing research and development since

1996. His research interests are in automatic target recognition, radar imaging and target tracking.